Kajal Sharma, Rajan Arora, Astha Chauhan* and Ashish Tiwari

Propagation of Waves in a Nonideal Magnetogasdynamics with Dust Particles

https://doi.org/10.1515/zna-2019-0255 Received August 3, 2019; accepted December 24, 2019; previously published online February 7, 2020

Abstract: In this article, we use the surface theory and compatibility conditions to describe the behaviour of wave propagation and their culmination into a shock wave in nonideal reacting gas with dust particles. The one-dimensional steepening of waves has been considered. A Bernoulli-type transport equation for the velocity gradient has been obtained. A numerical approach is used to explain the effects of van der Waals excluded volume of the medium, the ratio of specific heats, and the mass concentration of the solid particles on the shock wave.

Keywords: Breaking of Waves; Dusty Gas; Magnetic Field; Singular Surface Theory.

1 Introduction

Mathematicians and physicists have developed a great interest in the study of nonlinear waves because of its applications in many areas such as plasma physics, astrophysics, aerodynamics, nuclear science, etc. The field of shock waves has become very interesting not only because of its great scope in research area but also of its practical applications, as it is successfully used in medical field also. The investigation of shock waves is important for the point of view of research and practical applications.

The wave is considered as moving surface under which the variables and their derivatives undergo certain kind of discontinuities that are carried along by the surface. These discontinuities are bound to be interrelated. The relations that connect the field variables and their derivatives are known as compatibility conditions. These

*Corresponding author: Astha Chauhan, Department of Applied Science and Engineering, Indian Institute of Technology Roorkee, Roorkee, India, E-mail: asthaiitr1@gmail.com, achauhan1@as.iitr.ac.in. https://orcid.org/0000-0002-8995-2336 Kajal Sharma, Rajan Arora and Ashish Tiwari: Department of Applied Science and Engineering, Indian Institute of Technology Roorkee, Roorkee, India, E-mail: kajaliitr8@gmail.com (K. Sharma); rajanfpt@iitr.ac.in (R. Arora); ashish.tiwari41@gmail.com (A. Tiwari)

relations are defined along both sides of the discontinuity surface. These conditions have arisen because of the dynamical conditions that define the properties and behaviour of the material. The compatibility condition of first kind is known as Rankine-Hugoniot jump conditions. This set of compatibility conditions, which is a consequence of conservation laws, holds across the discontinuity surface. The relations between the first-order derivatives of the field variables on the two sides of the discontinuity surface and its speed of propagation are known as compatibility condition of first order. The compatibility conditions for the second- and higher-order derivatives can be obtained with the assumption of smooth wavefront. The geometrical and kinematical compatibility conditions of first and second order were developed by Thomas [1]. The growth and decay of discontinuities have been studied by Coleman and Gurtin [2]. When the wave steepened, the singular surface theory has been studied by Shyam et al. [3]. Chadha and Jena [4] investigated different modes of wave propagation using the compatibility conditions and singular surface theory suggested by Thomas.

When the energy of the electric field is much smaller than that of magnetic field, then all the electromagnetic quantities can be expressed in terms of magnetic field, and then only the interaction between gas-dynamic field and magnetic field can be considered. Such analysis is known as a magnetogasdynamics. Many investigators are interested in the propagation of shock waves influenced by strong magnetic field. Arora et al. [5] have studied the shock waves in magnetogasdynamics using similarity method. Pandey et al. [6] have obtained the exact solutions of magnetogasdynamics using Lie symmetry analysis. A detailed study on weak shock wave in nonideal magnetogasdynamics has been done by Nath et al. [7]. Chaturvedi et al. [8] described the evolution of weak shock wave in two-dimensional steady supersonic flow in dusty gas. The evolution of compression pulses in magnetohydrodynamics has been studied by Sharma [9]. The self-similar solutions of exponential shock waves and imploding shocks in nonideal magnetogasdynamics and the weak discontinuity in radiative magnetogasdynamics have been described by Singh et al. [10–14].

The study of fluid flow containing dust particles has grabbed undivided attentions by the researchers due to its wide applications in environmental and industrial fields such as lunar ash flow, nozzle flow, volcanic explosions, underground explosions, supersonic flight in the dusty air, the formation of polluted crystals, star formation, and many other problems of engineering. There are many research papers, which concern the study of the propagation of shock waves in the presence of dust particles. Chadha and Jena [15] have studied the propagation of waves in a dusty gas. Sahu [16] described the shock waves in rotational axisymmetry nonideal dusty gas. Yin et al. [17] studied the dusty shock numerically. The main motivation to work on magnetogasdynamics with dust particles is its application in astrophysics as dusty plasmas are common in astrophysical environments; examples range from the interstellar medium to cometary tails and planetary ring system. Where there are plasmas, there are charged particles zipping around, and thus, there are magnetic fields. Thus, the magnetic fields thread the planet and sun, the solar system, distant nebulas, and even the galaxy itself. Consolmagno [18] has shown the influence of the interplanetary magnetic field on cometary and primordial dust orbits. Morfill and Grün [19] described the motion in charged dust particles in interplanetary space. The change of the dust charge, when it is transferred from the region of weak magnetic field to the region of strong magnetic field, can be used in many experiments. The change of dust charges by magnetic fields is important in dust shocks, in strong magnetic fields where the value of the magnetic field suddenly changes at the surface of the shock.

Thus, the study of shock waves in magnetogasdynamics in dusty gas has great importance. Vishwakarma et al. [20] have obtained the self-similar solution for cylindrical shock waves in a weakly conducting dusty gas. The self-similar solutions of cylindrical shock wave in a dusty gas have been obtained by Chauhan and Arora [21]. Merlino et al. [22] have studied the nonlinear dust acoustic waves, shocks, and structures.

In this article, we considered a system of partial differential equations describing the planar and cylindrically symmetric flow in the presence of axial magnetic field. Employing the theory of singular surfaces, we study the various aspects of nonlinear wave propagation in a non-ideal medium in the presence of dust particles. In order to get some essential features of shock propagation, small solid particles are considered as a pseudofluid, and it is assumed that the equilibrium flow condition is maintained in the flow field and that the viscous stress and heat conduction of the mixture are negligible. There is no literature available to show these effects on magnetogasdynamics using singular surface theory as per the authors' knowledge. The density of the solid particles is much greater than the density of the gas. Therefore, the

volume occupied by the particles is negligible. The article is summarized as follows: in Section 1, a brief introduction about the magnetogasdynamics and shock waves is given. In Section 2, governing equations are described in brief, whereas in Section 3, the transport equation and the velocity of wave propagations are determined. Then, in Section 4 and 5, for a particular case, the behaviour of velocity gradient is discussed graphically, and then in Section 6, results and a brief conclusion are presented about the whole study. The effects of dust particles, van der Waals excluded volume, and the magnetic field strength on the shock wave propagation are investigated. All the computational work has been done using the software package MATLAB in which comparatively better approach viz. ode45 instead of Runge-Kutta and other methods has been used to obtain the solutions.

2 Governing Equations

The conservation equations governing the nonsteady onedimensional flow, which is the function of two independent variables, the space coordinate r and the time t, are as follows [23]:

$$\rho_{t} + \rho u_{r} + u \rho_{r} + \frac{(m-1)\rho u}{r} = 0,$$

$$u_{t} + u u_{r} + \frac{(p_{r} + h_{r})}{\rho} = 0,$$

$$E_{t} + u E_{r} - \frac{p}{\rho^{2}} (\rho_{t} + u \rho_{x}) = 0,$$

$$h_{t} + u h_{r} + 2h u_{r} + \frac{2h(m-1)u}{r} = 0,$$
(1)

where u, p, and ρ denote the velocity, pressure, and density, respectively. Magnetic pressure is denoted by h, which can be defined as $h=\frac{\sigma H^2}{2}$. Here, σ is the magnetic permeability, while H is the transverse magnetic field. For planar and cylindrically symmetric motion, m will assume the values 1 and 2, respectively. The internal energy E per unit mass of the mixture is defined as [24]:

$$E = \frac{(1-Z)p}{(\Gamma-1)(1+\tilde{b}\rho)\rho}.$$
 (2)

Here, Z denotes the volume fraction defined as

$$Z=rac{V_{sp}}{V_{\sigma}}$$
,

and k_p is the mass fraction in mixture defined as

$$k_p=\frac{m_{sp}}{m_{\sigma}}.$$

 V_{sp} is the volumetric extension, and m_{sp} is the total mass of solid particles. V_g is the total volume, while m_g is the total mass of the mixture.

$$\tilde{b}=b(1-k_n),$$

Its value lies between the range $0.9 \times 10^{-3} \le b \le 1.1 \times 10^{-3}$. Γ denotes the Grüneisen coefficient and is defined as $\Gamma = \frac{\gamma(1+\chi\beta)}{1+\chi\beta\gamma}$, where $\chi = \frac{k_p}{(1-k_p)}$ and β are the ratio of specific heat of solid particles at constant pressure (C_p) to the specific heat of gas at constant volume (C_v) . Also, we have the equation

$$Z=\frac{k_p}{(1-k_p)G+k_p},$$

where $G = \rho_{sp}/\rho_g$. Here, ρ_{sp} is the density of the solid particles, and ρ_g is the species density of the gas. Now, the equation of state is given as follows:

$$p=\frac{(1-k_p)(1+\tilde{b}\rho)}{(1-Z)}\rho RT,$$

where T and R denote the temperature and the specific gas constant, respectively. Thus, from (2), (1)₃ is transformed into

$$p_t + up_r + \rho a^2 \left(u_r + \frac{(m-1)u}{r} \right) = 0,$$

where a^2 is the equilibrium speed of sound, which is defined as

$$a^{2} = \left\lceil \frac{(\Gamma - \tilde{b}\mu\rho^{2} + 2\Gamma\tilde{b}\rho + (\Gamma - 1)\tilde{b}^{2}\rho^{2})p}{(1 - \mu\rho)(1 + \tilde{b}\rho)\rho} \right\rceil, \quad (3)$$

and depends on the parameter μ and b as follows:

Case 1: for $\mu = 0$ and b = 0, we have $\Gamma = \gamma$ and $a^2 = \frac{\gamma p}{\rho}$; mixture transforms into an ideal gas.

Case 2: for $\mu=0$ and $b\neq 0$, we have $\Gamma=\gamma$ and $a^2=\frac{p(\gamma+2\gamma\tilde{b}\rho+(\gamma-1)\tilde{b}^2\rho^2)}{\rho(1+\tilde{b}\rho)}$. Thus, mixture becomes a nonideal gas.

Case 3: for $\mu \neq 0$ and b = 0, we have $a^2 = \frac{\Gamma p}{\rho(1-\mu\rho)}$. Thus, it becomes a mixture of ideal gas and dust particles.

Case 4: for $\mu \neq 0$ and $b \neq 0$, a^2 is given by (3), which yields a mixture of dust particles and nonideal gas.

3 Velocity Gradient and Formation of the Transport Equation

We consider the equation of wavefront Ξ as

$$r=X(t), (4)$$

across which we have continuous flow variables ρ , u, p, and h, and the discontinuities in their derivatives are acceptable. Let A represent any of the flow variables ρ , u, p, or h with $\pi = \frac{\mathrm{d}X}{\mathrm{d}t}$, which is the propagation speed of Ξ , and Z and \tilde{Z} are the quantities defined on Ξ . Therefore, for a singular surface, the geometrical and kinematical compatibility conditions of first- and second-order are given by

$$|[A_r]| = Z, \quad |[A_t]| = -\pi Z,$$

 $|[A_{rr}]| = \tilde{Z}, \quad |[A_{rt}]| = \pi \left(\frac{\partial Z}{\partial r} - \tilde{Z}\right).$ (5)

Here, |[A]| denotes the jump in variable A across the surface Ξ , defined as $|[A]| = A - A_0$, where A_0 is the value just ahead of Ξ , and A denotes the value just behind the Ξ .

Let us consider

$$|[\rho_r]| = \theta, \quad |[u_r]| = \lambda, \quad |[p_r]| = \xi, \quad |[h_r]| = \eta, \quad (6)$$

thus,

$$|[\rho_t]| = -\pi\theta, \quad |[u_t]| = -\pi\lambda,$$

$$|[p_t]| = -\pi\xi, \quad |[h_x]| = -\pi\eta,$$
 (7)

Now, evaluating (1) on the inner boundary of $\boldsymbol{\Xi}$, we obtain

$$(\pi - u_0)\theta = \rho_0 \lambda, \quad (\pi - u_0)\rho_0 \lambda = \xi + \eta,$$

 $(\pi - u_0)\xi = a_0^2 \rho_0 \lambda, \quad (\pi - u_0)\eta = 2h_0 \lambda.$ (8)

Since π is positive for an advancing wave, the following relations are obtained between λ , η , θ , and ξ

$$\pi = Z_0 \rho_0 + u_0, \quad \lambda = Z_0 \theta = \frac{Z_0 \xi}{a_0^2} = \frac{Z_0 \rho_0 \eta}{2h_0},$$
 (9)

where

$$Z_0 = \left[\frac{1}{\rho_0} (a_0^2 + \frac{2h_0}{\rho_0})^{\frac{1}{2}} \right]. \tag{10}$$

Now, taking jump across Ξ after differentiating (1) with respect to r, we obtain

$$egin{aligned} &|[
ho_{rt}]|+
ho_0|[u_{rr}]|+2|[
ho_ru_r]|+u_0|[
ho_{rr}]|\ &+rac{1}{r}((m-1)
ho_0|[u_r]|)+rac{1}{r}((m-1)u_0|[
ho_r]|)=0,\ &|[u_{rt}]|+|[u_ru_r]|+u_0|[u_{rr}]|+rac{|[p_{rr}]|}{
ho_0}\ &+rac{|[h_{rr}]|}{
ho_0}-rac{|[
ho_rp_r]|}{
ho_0^2}-rac{|[
ho_rh_r]|}{
ho_0^2}=0, \end{aligned}$$

$$|[p_{rt}]| + u_{0}|[p_{rr}]| + \left(1 + \frac{\rho_{0}a_{0}^{2}}{p_{0}}\right)|[u_{r}\rho_{r}]|$$

$$+ \rho_{0}a_{0}^{2}\left(|[u_{rr}]| + \frac{(m-1)|[u_{r}]|}{r}\right)$$

$$+ \frac{p_{0}H_{0}|[u_{r}\rho_{r}]|}{(1 - \mu\rho_{0})^{2}(1 + \tilde{b}\rho_{0})^{2}}$$

$$+ \frac{(m-1)u_{0}}{r}\left(\frac{\rho_{0}a_{0}^{2}|[p_{r}]|}{p_{0}}\right)$$

$$+ \frac{p_{0}H_{0}|[\rho_{r}]|}{(1 - \mu\rho_{0})^{2}(1 + \tilde{b}\rho_{0})^{2}}\right) = 0,$$

$$|[h_{rt}]| + u_{0}|[h_{rr}]| + 3|[u_{r}h_{r}]| + 2h_{0}|[u_{rr}]|$$

$$+ \frac{1}{r}(2(m-1)h_{0}|[u_{r}]|)$$

$$+ \frac{1}{r}(2(m-1)u_{0}|[h_{r}]|) = 0,$$
(11)

where

$$H_{0} = (1 - \mu \rho_{0})(1 + \tilde{b}\rho_{0})$$

$$\{2\tilde{b}\Gamma - 2\mu \rho_{0}\tilde{b} + 2(\Gamma - 1)\tilde{b}^{2}\rho_{0}\}$$

$$-\{\Gamma - \tilde{b}\mu \rho_{0}^{2} + 2\Gamma\tilde{b}\rho_{0} + (\Gamma - 1)\tilde{b}^{2}\rho_{0}^{2})\}$$

$$(\tilde{b} - \mu - 2\tilde{b}\mu\rho_{0}). \tag{12}$$

Using (5), (6), and

$$|[\rho_{rr}]| = \tilde{\theta}, \quad |[u_{rr}]| = \tilde{\lambda},$$

$$|[p_{rr}]| = \tilde{\xi}, \quad |[h_{rr}]| = \tilde{\eta}, \quad (13)$$

and

$$|[\rho_{rt}]| = \pi(\theta_r - \tilde{\theta}), \quad |[u_{rt}]| = \pi(\lambda_r - \tilde{\lambda}),$$

$$|[p_{rt}]| = \pi(\tau_r - \tilde{\tau}), \quad |[h_{rt}]| = \pi(\eta_r - \tilde{\eta}).$$
 (14)

in (11), we get

$$\begin{split} \pi(\theta_{r} - \tilde{\theta}) + \rho_{0}\tilde{\lambda} + 2(\theta\lambda + \rho_{0_{r}}\lambda + u_{0_{r}}\theta) \\ + u_{0}\tilde{\theta} + \frac{1}{r}((m-1)\rho_{0}\lambda) + \frac{1}{r}((m-1)u_{0}\theta) &= 0, \\ \pi(\lambda_{r} - \tilde{\lambda}) + (\lambda^{2} + 2u_{0_{r}}\lambda) + u_{0}\tilde{\lambda} + \frac{\tilde{\eta}}{\rho_{0}} + \frac{\tilde{\xi}}{\rho_{0}} \\ - \frac{1}{\rho_{0}^{2}}(\theta\xi + p_{0_{r}}\theta + \rho_{0_{r}}\xi) \\ - \frac{1}{\rho_{0}^{2}}(\eta\theta + h_{0_{r}}\theta + \rho_{0_{r}}\eta) &= 0, \\ \pi(\xi_{r} - \tilde{\xi}) + u_{0}\tilde{\xi} + \left(1 + \frac{\rho_{0}a_{0}^{2}}{p_{0}}\right)(\lambda\xi + u_{0_{r}}\xi + p_{0_{r}}\lambda) \\ + \rho_{0}a_{0}^{2}\left(\tilde{\lambda} + \frac{(m-1)\lambda}{r}\right) \end{split}$$

$$+ \frac{p_0 H_0}{(1 - \mu \rho_0)^2 (1 + \tilde{b} \rho_0)^2} (\lambda \theta + u_{0_r} \theta + \rho_{0_r} \lambda)$$

$$+ \frac{(m - 1) u_0}{r} \left(\frac{\rho_0 a_0^2 \xi}{p_0} + \frac{p_0 H_0 \theta}{(1 - \mu \rho_0)^2 (1 + \tilde{b} \rho_0)^2} \right)$$

$$= 0,$$

$$\pi (\eta_r - \tilde{\eta}) + u_0 \tilde{\eta} + 3(\lambda \eta + u_{0_r} \eta + h_{0_r} \lambda)$$

$$+ 2h_0 \tilde{\lambda} + \frac{1}{r} (2(m - 1) h_0 \lambda)$$

$$+ \frac{1}{r} (2(m - 1) u_0 \eta) = 0.$$
(15)

After eliminating $\tilde{\eta}$, $\tilde{\theta}$, and $\tilde{\xi}$, and using (9), (15), and $\pi = Z_0 \rho_0 + u_0$, Bernoulli type of transport equation for λ is obtained as follows:

$$2\frac{\mathrm{d}\lambda}{\mathrm{d}t} + \Sigma_1\lambda + \Sigma_2\lambda^2 = 0, \tag{16}$$

where

$$\Sigma_{1} = 3u_{0_{r}} + \frac{3\rho_{0}Z_{0}h_{0_{r}}}{2h_{0}} + \frac{2(m-1)}{r} \left(u_{0} + \frac{Z_{0}\rho_{0}}{2}\right)$$

$$+ \left(1 + \frac{\rho_{0}a_{0}^{2}}{p_{0}}\right) \left(u_{0_{r}} + \frac{Z_{0}p_{0_{r}}}{a_{0}^{2}}\right) + \frac{mZ_{0}\rho_{0}}{r}$$

$$+ \frac{H_{0}p_{0}}{(1 - \mu\rho_{0})^{2}(1 + \tilde{b}\rho_{0})^{2}} \left(\frac{Z_{0}\rho_{0_{r}}}{a_{0}^{2}} + \frac{u_{0_{r}}}{a_{0}^{2}}\right)$$

$$+ \frac{mu_{0}}{r} \left(\frac{a_{0}^{2}\rho_{0}}{p_{0}} + \frac{H_{0}p_{0}}{(1 - \mu\rho_{0})^{2}(1 + \tilde{b}\rho_{0})^{2}a_{0}^{2}},\right)$$

$$\Sigma_{2} = 4 + \frac{\rho_{0}a_{0}^{2}}{p_{0}} + \frac{p_{0}H_{0}}{(1 - \mu\rho_{0})^{2}(1 + \tilde{b}\rho_{0})^{2}a_{0}^{2}}.$$
(17)

The amplitude of the acceleration waves, also known as discontinuity waves characterized by a discontinuity in a normal derivative of the field, satisfies a transport equation of Bernoulli type. One can easily find a brief explanation of the discontinuity waves and its applications from [25–30] and conclude that the transport equation for the discontinuities follows the Bernoulli-type equation.

4 Particular Case

To obtain the value of λ , we need the values of flow parameters p_0 , ρ_0 , u_0 , and h_0 ahead of wavefront Ξ . We consider the following form of values:

$$u_0(x, t) = y(t)r, \quad \rho_0 = \rho_0(t),$$

 $p_0 = p_0(t), \quad h_0 = h_0(t),$ (18)

where the particle velocity linearly depends on the spatial coordinate at equilibrium state. This state can be visualized in terms of an atmosphere filled with a gas, which has the spatially uniform pressure variations on account of particle motion [31].

In view of (18), we integrate (1) to obtain the values of ρ_0 , p_0 , u_0 , and u_0 as

$$y(t) = y_{0c} \{ 1 + (t - t_{0c})y_{0c} \}^{-1},$$
 (19)

$$\rho_0(t) = \rho_{0c} \{ 1 + (t - t_0) y_{0c} \}^{-m}, \tag{20}$$

$$h_0(t) = h_{0c} \{ 1 + (t - t_{0c}) y_{0c} \}^{-2m},$$
 (21)

$$p_{0} = p_{0c} \{1 + y_{0c}(t - t_{c})\}^{\frac{-m(\Gamma \mu - \tilde{b})}{(\mu - \tilde{b})}}$$
$$(1 - \tilde{b}\rho_{0})^{-1} (1 - \mu\rho_{0})^{\frac{-(\Gamma \mu - \tilde{b})}{(\mu - \tilde{b})}}, \tag{22}$$

where y_{0_c} , ρ_{0_c} , and h_{0_c} denote the reference values of the flow variables velocity, density, and magnetic pressure, respectively, at $t = t_c$.

5 Behaviour of the Velocity Gradient

Now, we consider the following dimensionless variables to compute the velocity gradient:

$$r_{0}^{*} = \frac{r_{0}}{t_{0_{c}} a_{0_{c}}}, \quad t^{*} = \frac{t}{t_{0_{c}}}, \quad y^{*} = y t_{0_{c}}, \quad \rho_{0}^{*} = \frac{\rho_{0}}{\rho_{0_{c}}},$$

$$p_{0}^{*} = \frac{p_{0}}{\rho_{0_{c}} a_{0_{c}}^{2}}, \quad h_{0}^{*} = \frac{h_{0}}{\rho_{0_{c}} a_{0_{c}}^{2}}, \quad a_{0}^{*} = \frac{a_{0}}{a_{0_{c}}},$$

$$b^{*} = \rho_{0c} b, \quad \lambda^{*} = t_{0c} \lambda. \tag{23}$$

Using (23), we obtain the transport (16) after suppressing the asterisk sign as follows:

$$2\frac{d\lambda}{dt} + \phi_1 \lambda + \phi_2 \lambda^2 = 0,$$

$$\phi_1 = 3y + \frac{3h_{0r}\rho_0 Z_0}{2h_0} + \frac{2(m-1)}{r} \left(u_0 + \frac{Z_0\rho_0}{2} \right)$$

$$+ \left(1 + \frac{\rho_0 a_0^2}{p_0} \right) y + \frac{mZ_0\rho_0}{r}$$

$$+ \frac{H_0 p_0 y}{(1 - \mu\rho_0)^2 (1 + \tilde{b}\rho_0)^2 a_0^2}$$

$$+ my \left(\frac{a_0^2 \rho_0}{p_0} + \frac{H_0 p_0}{(1 - \mu\rho_0)^2 (1 + \tilde{b}\rho_0)^2 a_0^2} \right),$$

$$\phi_2 = 4 + \frac{\rho_0 a_0^2}{p_0} + \frac{p_0 H_0}{(1 - \mu\rho_0)^2 (1 + \tilde{b}\rho_0)^2 a_0^2}.$$
(24)

Integrating (16) with respect to t, we obtain the value of λ as follows:

$$\lambda = \frac{\lambda_0 \psi_1(t)}{1 + \lambda_0 \psi_2(t)},\tag{25}$$

where $\psi_2 = \int_{t_0}^t \phi_1(s)\psi_1(s)ds$, $\psi_1 = \exp(-\int_{t_0}^t \phi_2(s)ds)$, and $\lambda_0 = \lambda(t_0)$. From (25), it may be noted that at some critical time $t = t_c$ where $1 + \lambda_0 \psi_2(t) = 0$, the solution (25) breaks down. This indicates the presence of an acceleration wave at an instant t_c , i.e. a compression wave culminates into a shock in a finite time t_c only when the initial discontinuity associated with the wave becomes more than a critical value. Numerical integration of (25) is carried out using (19–22) for $1 \le t < \infty$ to study the effects of nonideal gas, dust particles, and the initial magnetic field on the jump discontinuity $[u_r]$, and the results are depicted graphically in Figures 1-6. Parameters of the mixture (alumina Al₂O₃ or glass) are within the following range: dust particle size is in the order of 1-10 µm, the material density of solid particles $\rho_{sp} = 2.5 \text{g/cm}^3$, and the mass fraction (concentration) of solid particles in the mixture is varied from $k_p = 0.0$ to $k_p = 0.6$. This case may be realized in an air flow with a suspension of alumina or glass particles. The diameter of small solid particles used in the present study $d = 10 \mu m$ is larger than the shock wave thickness, which is of the order of 0.066 µm. It can be assumed that the small solid particles are unaffected when they pass through the shock fronts. Also, the particle size 1–10 µm corresponds to interplanetary dust. The values involved for computation are taken as $h_{0c} = 0.01$, $\beta = 1$, $k_p = 0.6$, G = 1000, b = 0.0009, and $\gamma = 1.4$. The values $\beta = 1$, $\gamma = 1.4$ may correspond to the mixture of

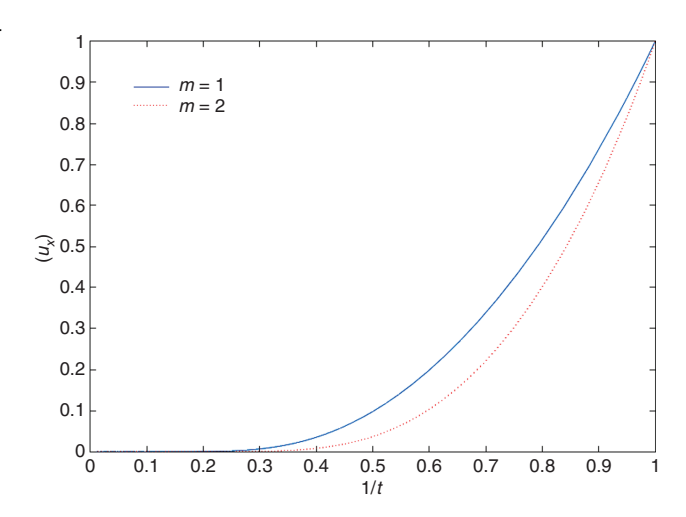


Figure 1: Flow profiles of velocity gradient $[u_r]$ for different values of m with $k_0=0.1$, $\beta=1.0$, $k_p=0.6$, G=1000, $\beta=1.0$, $y_{0_c}=0.1$, $\rho_{0_c}=100$, $\rho_{0_c}=0.01$, $h_{0_c}=0.01$, and $\gamma=1.4$.

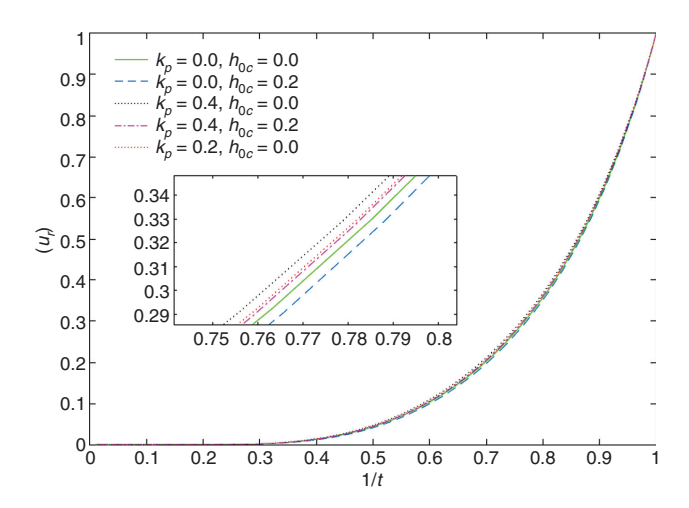


Figure 2: Flow profiles of velocity gradient $[u_r]$ for different values of k_p with $k_0=0.1$, $\beta=1.0$, b=0.0009, G=1000, $y_{0_c}=0.1$, $\rho_{0_c}=100$, $\rho_{0_c}=0.01$, $h_{0_c}=0.01$, and $\gamma=1.4$.

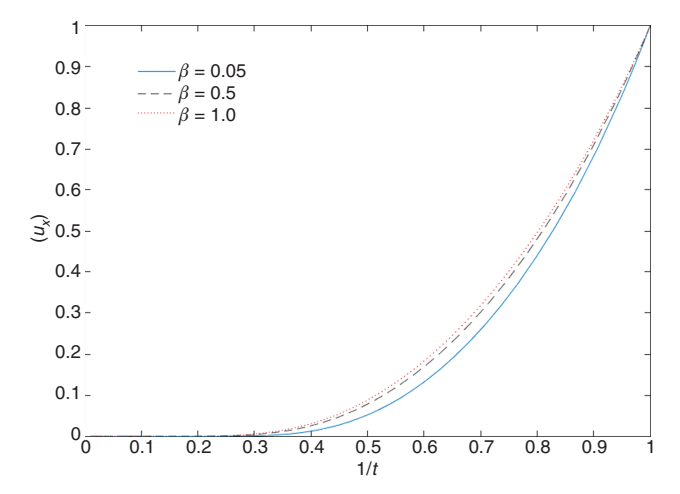


Figure 3: Flow profiles of velocity gradient $[u_r]$ for different values of β with $k_0 = 0.1$, $k_p = 0.6$, b = 0.0011, G = 1000, $y_{0_c} = 0.1$, $\rho_{0_c} = 100$, $\rho_{0_c} = 0.01$, $h_{0_c} = 0.01$, and $\gamma = 1.4$.

glass particles. When G=10, small solid particles of density equal to 10 times that of the perfect gas in the mixture occupy a significant portion of the volume, which lowers the compressibility of the medium remarkably. Then, an increase in k_p further reduces the compressibility, which causes an increase in the distance between the shock front and the piston and a decrease in the shock strength. In the case of G=100, small solid particles of density equal to 100 times that of the perfect gas in the mixture occupy a very small portion of the volume, and therefore compressibility is not lowered much, but the inertia of the mixture is increased significantly due to the particle load. An increase in k_p from 0.2 to 0.4 for G=100 means that the perfect gas in the mixture constituting 80% of the total

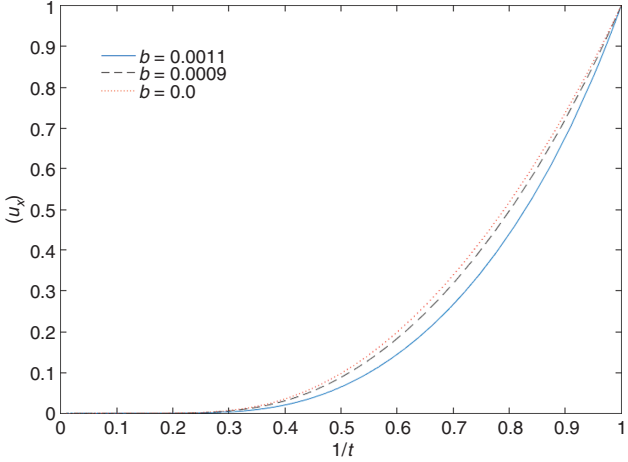


Figure 4: Flow profiles of velocity gradient $[u_r]$ for different values of b with $k_0=0.1$, $\beta=1.0$, $k_p=0.6$, G=1000, $y_{0_c}=0.1$, $\rho_{0_c}=100$, $\rho_{0_c}=0.01$, $h_{0_c}=0.01$, and $\gamma=1.4$.

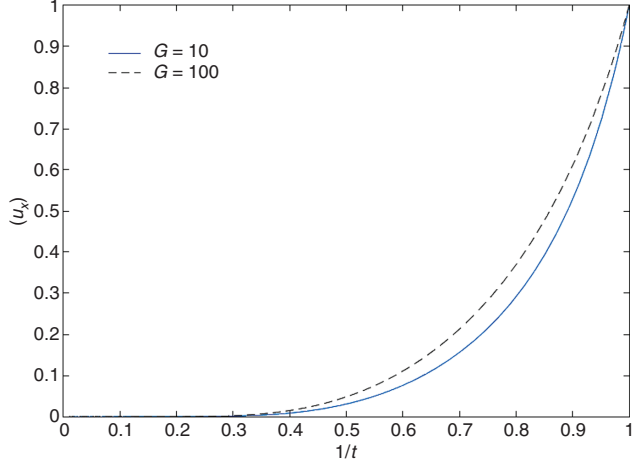


Figure 5: Flow profiles of velocity gradient $[u_r]$ for different values of G with $k_0=0.1$, $\beta=1.0$, $k_p=0.6$, b=0.0011, $y_{0_c}=0.1$, $\rho_{0_c}=100$, $\rho_{0_c}=0.01$, $h_{0_c}=0.01$, and $\gamma=1.4$.

mass and occupying 99.75% of the total volume now constitutes 60% of the total mass and occupies 99.34% of the total volume. Due to this fact, the density of the perfect gas in the mixture is highly decreased, which overcomes the effect of incompressibility of the mixture. The same case can be considered for G=1000. For a detailed study, one can follow [20]. The obtained numerical solutions are consistent with the asymptotic results in the neighbourhood of $t=\infty$. From Figures 1 to 6, it is observed that λ goes up as t goes down and tends to zero as t tends to infinity.

Figure 1 shows the variation of the velocity gradient with different values of m. Figures 2–6 show the effects of parameters β , b, G, k_p , and h_0 on λ for m=1. An increment in the value of the parameters k_p , β , and G gives a rise in velocity gradient λ , and an increment in the value of the

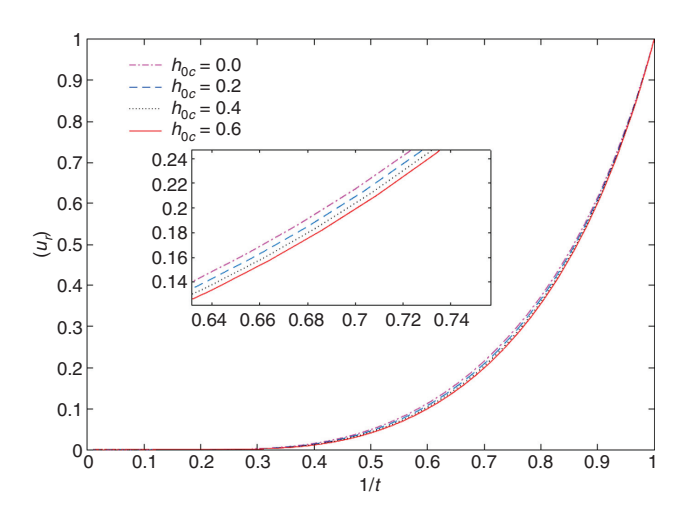


Figure 6: Flow profiles of velocity gradient $[u_r]$ for different values of h_0 with $k_0 = 0.1$, $\beta = 1.0$, $k_p = 0.6$, b = 0.0011, G = 1000, $y_{0_c} = 0.1$, $p_{0_c} = 100$, $p_{0_c} = 0.01$, and $p_{0_c} = 0.4$.

parameter of nonidealness b causes a decrement in λ . An increase in the initial magnetic field leads to a decrease in the velocity gradient λ .

6 Results and Conclusion

In this article, the evolutionary behaviour of steepening of waves in a dusty gas in the presence of axial magnetic field is studied. It is observed that the jumps in the gradient of flow variables such as jumps in velocity gradient, pressure gradient, and density gradient are related. With the help of compatibility conditions and singular surface theory, the transport equation for jump in velocity gradient has been evaluated for the particular case, where the velocity at equilibrium reference state is considered to be linearly dependent on the spatial coordinate. A Bernoullitype equation has been satisfied by the jump in velocity gradient. From the analytic solution of the obtained transport equation, it is observed that for $\lambda_0 > 0$, $\lambda(t)$ tends to zero as t tends to infinity, which implies that the shock wave decays and dies out eventually. However, $\lambda_0 < 0$ implies that the solution (25) breaks down at some critical time $t = t_c$, where $1 + \lambda_0 \psi_2(t) = 0$. This instantly indicates the formation of a shock wave at t_c . For the gases with different values of the parameters b, β , K_p , and G, the time required for this breakdown is not the same. The time required for the formation of shock decreases as b and initial magnetic field increase and decreases as the value of any of the parameters β , K_p , and G increase.

Figure 1 represents the variation of $[u_r]$ with planar (m = 1) and cylindrical (m = 2) symmetry. It is observed that the velocity gradient decreases as m increases and

tends to zero at a faster rate. Also, the velocity gradient slows down as t goes up and tends to zero as t tends to infinity. From Figure 2, it may be concluded that as the value of the parameter k_p increases without the presence of magnetic field, the velocity gradient increases, which shows the same behaviour of results reported by Chadha and Jena [15], and when $k_p = 0$, it is observed that as the value of initial magnetic field h_{0c} increases, the velocity gradient decreases, which shows the same behaviour of $[u_r]$ reported in [32]. The effects of nonidealness parameters β , b, and G for cylindrically symmetric flow on shock formation are shown graphically through Figures 3-5. As the values of the parameters β and G increase, the flow profile of $\lambda = [u_r]$ increases, whereas an increment in the value of b leads to a fall in λ . Figure 6 represents that as the initial magnetic field increases, the velocity gradient decreases. On the basis of all the obtained results shown in Figures 1–6, it may be concluded that our results are in good agreement with the results reported in [15] and [33].

The potential applications of shock wave in magnetogasdynamics in a dusty gas are in active rocket experiments in near-Earth space and production of transient atmospheres of atmosphere-less cosmic bodies (Moon, Mercury, asteroid, and comet) as a result of impacts of large meteoroids or manmade projectiles with these bodies. This study can also be related to some questions being investigated in astrophysical plasmas as follows:

Shocks from supernova explosions – The layer of dust behind the supernova shock is observed usually. The problem is to verify whether the layer of dust is related to the process of dust condensation behind the shock wavefront.

Star formation in shocked molecular clouds – One believes that most of new stars are formed in dust-molecular clouds, and shock waves initiate this process. They create an increase in density sufficient for the gravitational self-compression (Jeans instability). The observations show that the presence of dust is well correlated with star formations. In particular, there are direct observations of star formation in dusty clouds.

Acknowledgements: The first author, Kajal Sharma, acknowledges the financial support awarded by the Department of Science and Technology, New Delhi, under the scheme Junior Research Fellowship. The corresponding author, Astha Chauhan, is thankful to the University Grant Commission, New Delhi, for financial support with grant number 2121440656 (Ref. No. 21/12/2014(ii)EU-V).

References

- [1] T. Y. Thomas, Int. J. Eng. Sci. 4, 207 (1966).
- [2] B. D. Coleman and M. E. Gurtin, J. Chem. Phys. 47, 597 (1967).
- [3] R. Shyam, L. P. Singh, and V. D. Sharma, Acta Astronaut. 13, 95 (1986).
- [4] M. Chadha and J. Jena, Comput. Appl. Math. 34, 729 (2015).
- [5] R. Arora, S. Yadav, and M. J. Siddiqui, Bound. Value Probl. 2014, 142 (2014).
- [6] M. Pandey, R. Radha, and V. D. Sharma, Q. J. Mech. Appl. Math. 61, 291 (2008).
- [7] T. Nath, R. K. Gupta, and L. P. Singh, Acta Astronaut. 133, 397
- [8] R. K. Chaturvedi, P. Gupta, and L. P. Singh, Acta Astronaut. 160, 552 (2019).
- [9] V. D. Sharma, Q. J. Mech. Appl. Math. 40, 527 (1987).
- [10] L. P. Singh, S. D. Ram, and D. B. Singh, Meccanica 48, 841 (2013).
- [11] L. P. Singh, M. Singh, and A. Husain, Astrophys. Space Sci. **331**, 597 (2011).
- [12] L. P. Singh, A. Husain, and M. Singh, Meccanica 46, 437 (2011).
- [13] L. P. Singh, M. Singh, and B. D. Pandey, AIAA J. 48, 2523 (2010).
- [14] L. P. Singh, A. Husain, and M. Singh, Acta Astronaut. 68, 16 (2011).

- [15] M. Chadha and J. Jena, Int. J. Nonlinear Mech. 74, 18 (2015).
- [16] P. K. Sahu, Phys. Fluids 29, 086102 (2017).
- [17] J. Yin, J. Ding, and X. Luo, Phys. Fluids 30, 013304 (2018).
- [18] G. J. Consolmagno, Icarus 43, 203 (1980).
- [19] G. E. Morfill and E. Grün, Planet. Space Sci. 27, 1269 (1979).
- [20] J. P. Vishwakarma, G. Nath, and R. K. Srivastava, Ain Shams Eng. J. 9, 1717 (2018).
- [21] A. Chauhan and R. Arora, Indian J. Phys. 1, 2019. https://doi.org/10.1007/s12648-019-01499-3.
- [22] R. L. Merlino, J. R. Heinrich, S. H. Kim, and J. K. Meyer, Plasma Phys. Control. F. 54, 124014 (2012).
- [23] M. J. Siddiqui, R. Arora, and A. Kumar, Chaos Soliton. Fract. 97, 66 (2017).
- [24] J. P. Vishwakarma and G. Nath, Meccanica 44, 239 (2009).
- [25] W. Bleakney and A. H. Taub, Rev. Mod. Phys. 21, 584 (1949).
- [26] G. Boillatt and T. Ruggeri, P. Roy. Soc. Edinb. A 83, 17 (1979).
- [27] A. Jeffrey, Quasilinear Hyperbolic Systems and Waves, Pitman Publishing, London 1976, p. 230.
- [28] A. Jeffrey, Appl. Anal. 3, 79 (1973).
- [29] A. Mentrelli, T. Ruggeri, M. Sugiyama, and N. Zhao, Wave Motion 45, 498 (2008).
- [30] V. D. Sharma, Int. J. Eng. Sci. 24, 813 (1986).
- [31] V. D. Sharma, R. Ram, and P. L. Sachdev, J. Fluid Mech. 185, 153 (1987).
- [32] S. Mehla and J. Jena, Rocky Mt. J. Math. 49, 235 (2019).
- [33] R. Singh and J. Jena, Int. J. Nonlinear Mech. 77, 158 (2015).